J. Fluid Mech. (2021), *vol*. 926, A32, doi:10.1017/jfm.2021.738

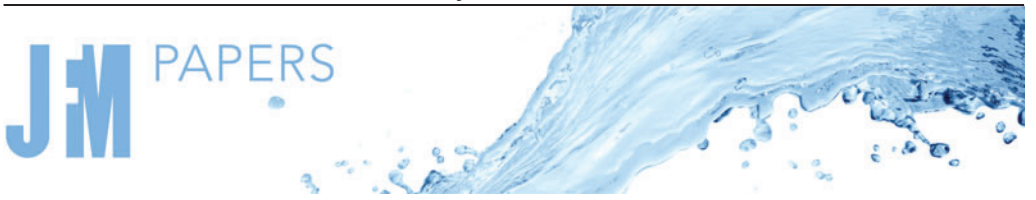

Buoyancy-driven instabilities of partially miscible fluids in inclined porous media

Hamid Emami-Meybodi[1],† **and Fengyuan Zhang**[2]

[1]Department of Energy and Mineral Engineering and EMS Energy Institute, Pennsylvania State University, University Park, PA 16802, USA

[2]Department of Oil and Gas Field Development Engineering, China University of Petroleum, Beijing 102249, PR China

(Received 19 May 2020; revised 4 August 2021; accepted 16 August 2021)

This study presents a buoyancy-driven stability analysis in a three-dimensional inclined porous medium with a capillary transition zone that is formed between a non-wetting and an underlying wetting phase. In this two-phase, two-component, partially miscible system, a solute from a non-wetting phase diffuses into a porous layer saturated with a wetting-phase fluid, creating a dense diffusive boundary layer beneath an established capillary transition zone. Transient concentration and gravity-driven velocity fields are derived for the wetting phase while the saturation field remains fixed. Linear stability analysis with the quasi-steady-state approximation is employed to determine the onset of solutal convective instability for buoyancy-dominant, in-transition and capillary-dominant systems. The analysis of the problem leads to a differential eigenvalue problem composed of a system of three complex-valued equations that are numerically solved to determine the critical times, critical wavenumbers and neutral stability curves as a function of inclination angle for different Bond numbers. The layer inclination is shown to play an essential role in the stability of the problem, where the gravity-driven flow removes solute concentrations in the diffusive boundary layer. The results indicate that the horizontal porous layer exhibits the fastest onset of instability, and longitudinal rolls are always more unstable than oblique and transverse rolls. The inclination angle has a more substantial impact on stabilizing the diffusive boundary layer in the buoyancy-dominant than in the capillary-dominant systems. Furthermore, for both buoyancy-dominant and capillary-dominant systems, the critical times and wavenumbers vary exponentially with inclination angle $\leq 60^\circ$ and follow the Stirling model.

Key words: buoyancy-driven instability, natural convection, inclined porous media

† Email address for correspondence: emami@psu.edu

1. Introduction

Buoyancy-driven convection of a diffusive boundary layer induced by concentration gradients is a subject widely explored in the literature (Riaz *et al.* 2006; Slim 2014; Emami-Meybodi *et al.* 2015). The typical set-up giving rise to unstable behaviour is one where the vertical transient concentration gradient is directed downwards. Such Darcy–Bénard-like configuration pertains to a diffusive boundary layer that grows with time and becomes gravitationally unstable under certain circumstances. The evolution of instabilities forms the fingers of a dense fluid penetrating into a lighter underlying fluid, which results in natural convection. This convective mixing significantly enhances the rate of mass transfer, rather than relying on slow mass transfer by diffusion.

Much research has been done to investigate the buoyancy-driven convection in fluid-saturated porous media since the pioneering work of Horton & Rogers (1945) and Lapwood (1948) for thermal convection. Most of the studies investigating thermoconvective instability of a motionless base state are related to a horizontal layer with impermeable and isothermal walls kept at different temperatures, which is known as the Darcy–Bénard problem (Nield & Bejan 2017). The Darcy–Bénard problem has been extended to an inclined porous layer in the pioneering studies by Bories & Combarnous (1973) and Weber (1974). The main consequence of the layer inclination is that the base state would have a stationary and parallel buoyant flow with a zero mass flow rate. Recent studies have shed light on the instability of the Darcy–Bénard problem in inclined systems (Rees & Bassom 2000; Rees, Storesletten & Postelnicu 2006; Barletta & Storesletten 2011; Sphaier, Barletta & Celli 2015).

The solutal convective instability has received significant attention over the past two decades due to its application to the storage of carbon dioxide (CO_2) in deep saline aquifers (Hassanzadeh, Pooladi-Darvish & Keith 2005; Bolster 2014; Emami-Meybodi *et al.* 2015). Most studies examined the process of solute convection in a Darcy–Bénard-like configuration for a horizontal layer with a Dirichlet-type boundary condition for the solute concentration while imposing zero flux at the top and assuming single-phase flow. This simplification ignores the capillary transition zone that may exist between two partially miscible fluids, i.e. the non-wetting CO_2 phase and the wetting water phase. The capillary transition zone allows the vertical flow of the diffusive boundary layer, potentially decreasing the onset time of instability. The effects of the capillary transition zone on solutal convective instabilities have been studied by using either a permeable upper boundary condition in a single-phase system (Slim & Ramakrishnan 2010; Elenius, Nordbotten & Kalisch 2012; Kim 2015) or a transition zone in a two-phase system (Emami-Meybodi & Hassanzadeh 2013; Emami-Meybodi 2017; Zhang & Emami-Meybodi 2018). In all these studies, a perfectly horizontal porous layer is considered to examine the solutal convection instability of a motionless base state.

This study aims to go beyond the analysis of two-phase buoyancy-driven flow in a horizontal porous layer by devising an inclined set-up where a capillary transition zone is formed between a non-wetting and a denser wetting phase. In particular, the critical role of the layer inclination on the onset of instability is examined for buoyancy-dominant, in-transition and capillary-dominant systems. The diffusion of solute from the non-wetting phase into the underlying wetting region may increase the density of the wetting phase and create a gravitationally unstable diffusive boundary layer beneath the capillary transition zone. While the dense diffusive boundary layer can potentially create solutal convective instabilities, the gravity-driven flow that arises from the variation of wetting-phase density across the inclined porous layer may delay the onset of natural convection. Hence, the base

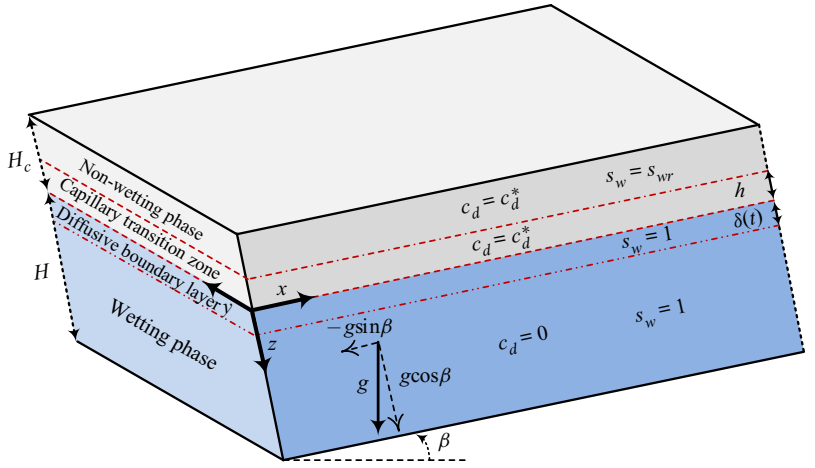

Figure 1. Geometry and coordinates of the inclined three-dimensional two-phase, two-component, partially miscible system with a capillary transition zone h formed between the wetting and non-wetting phases. The capillary transition zone and the underlying wetting-phase region ($-h \leq z \leq H$) are considered to conduct linear stability analysis. At time zero, the wetting phase in the capillary transition zone is saturated with the diffusive species $c_d = c_d^*$ (grey shaded area), while the wetting-phase domain is free of solute concentration $c_d = 0$ (blue shaded area). Solute gradually diffuses into the wetting-phase region and creates a diffusive boundary layer with a penetration depth of $\delta(t)$. As the diffusive boundary layer grows with time, it becomes denser and may result in natural convection.

state of the problem under consideration deals with transient concentration and through flow profiles. Details about the system under consideration are described in § 2.1 (see figure 1).

The analysis to be carried out is an extension of the work by Emami-Meybodi & Hassanzadeh (2013) and Zhang & Emami-Meybodi (2018) with reference to the special case of a two-dimensional horizontal layer. This analysis considers a three-dimensional, two-phase (e.g. supercritical CO_2 as non-wetting phase and brine as the wetting phase), two-component (e.g. CO_2 and H_2O) system in an inclined saturated porous medium, which is further described in § 2. In that section, the governing equations and the boundary conditions are also discussed. The dimensional analysis presented therein demonstrates that the two-phase, partially miscible, inclined system under consideration can be explored with five parameters, namely: viscosity ratio, gravity number, material parameter, Bond number and inclination angle. Section 3 provides the base state solutions for the saturation, velocity and concentration fields, around which the model is linearized. This includes a new time–space flow equation for the gravity-driven flow of the wetting phase through the porous medium. Section 3 also presents the linear stability formulations and discusses the quasi-steady-state approximation and the computational techniques that are used to solve a differential eigenvalue problem composed of a system of three complex-valued equations. Section 4 discusses the results of the linear stability analysis and shows the stabilizing effect of the inclination angle for different systems with different Bond numbers. The results obtained herein reveal the critical role of inclination angle on the stability of a diffusive boundary layer in the presence of a capillary transition zone and cast new light on future investigations concerning the stability of convective flow systems. Finally, § 5 summarizes the main conclusions of the present study.

2. Mathematical model

2.1. *Conceptual model*

During the active phase of CO_2 injection into a deep saline aquifer, CO_2 is forced radially outwards, assuming a vertical completion of injection wells. Away from the wells, CO_2 rises due to buoyancy and spreads out to form a thin plume beneath the overlying caprock. The plume then continues to migrate in horizontal directions (x- and y-directions). To make theoretical progress, most previous theoretical studies (Ennis-King & Paterson 2005; Riaz *et al.* 2006; Hassanzadeh, Pooladi-Darvish & Keith 2007; Ghesmat, Hassanzadeh & Abedi 2011; Slim 2014; Daniel, Riaz & Tchelepi 2015; Emami-Meybodi *et al.* 2015) make two simplifications. The first simplification is to recognize that the time scales for diffusion and free convection to become significant are typically much longer than the time for the injection phase and the establishment of a plume beneath the caprock. Even for a plume migrating updip, which could be slow for small updip angles, local CO_2 saturation will still be typically stabilized much more quickly than free convection can be established. The second common simplification is to consider an infinite lateral extent for the CO_2 plume because the length and width of the CO_2 plume are significantly larger than the size of natural convection cells. Thus, our analysis begins with CO_2 distributed in a laterally very extensive plume (i.e. the lateral extents in both x- and y-directions are infinite) of constant thickness spread beneath the caprock, assuming that the processes that created that distribution are faster than those examined in this study.

We considered an inclined three-dimensional, two-phase (i.e. wetting phase and non-wetting phase), two-component system (solute in the non-wetting phase and solvent in the wetting phase), as depicted figure 1. The inclined porous layer has an inclination angle of $\beta \in [0°, 90°]$ to the horizontal. We assumed that the saturated porous medium is non-deformable, isotropic and homogeneous with a height of $H + H_c$, where H_c and H are the heights of the gas cap and wetting-phase layer, respectively. A capillary transition zone with a height of h was considered between the wetting and non-wetting phases because of gravity–capillary equilibration. The solute in the gas cap diffuses into the underlying porous layer saturated with the wetting phase. A Cartesian coordinate system was chosen, in which the x-axis is along the porous medium and the z-axis is positive downwards. The origin of the space coordinates is at the interface between H_c and H. The capillary transition zone combined with the underlying wetting-phase region ($-h \le z \le H$) was considered as the domain of study. In this domain, gravity is oriented downwards and deviates from the z-axis by β. The lower boundary of the domain was considered to be impermeable with zero mass flux and the upper boundary was maintained at constant pressure ($p = p_i$) and concentration ($c_d = c_d^*$), where c_d^* is the maximum concentration of the diffusive species in the wetting phase. At time zero, the wetting-phase domain was free of solute concentration ($c_d = 0$). We assumed that the Boussinesq approximation and Darcy's law are valid.

2.2. *Governing equations*

The governing equations to describe the two-phase system are given by the multiphase extension of Darcy's law, the convection–diffusion equation and the continuity equations (Aziz & Settari 1979; Chen, Huan & Ma 2006):

$$\boldsymbol{v}_l = -\frac{k k_{rl}}{\mu_l}(\nabla p_l - \rho_l g \nabla z), \quad l = n, w, \tag{2.1a}$$

$$\phi \frac{\partial}{\partial t} \sum_{l=n,w} s_l \rho_l c_{dl} = -\nabla \cdot \sum_{l=n,w} (\boldsymbol{v}_l c_{dl} - \phi s_l D_{0l} \nabla c_{dl}), \tag{2.1b}$$

$$\varphi \frac{\partial}{\partial t} \sum_{l=n,w} s_l \rho_l + \nabla \cdot \sum_{l=n,w} \rho_l \boldsymbol{v}_l = 0. \tag{2.1c}$$

These are constrained by the following relations:

$$s_n + s_w = 1, \quad p_c = p_n - p_w. \tag{2.2a,b}$$

In the above equations, $\boldsymbol{v} = [u, v, w]$ is the Darcy velocity vector, u, v and w are the velocity components in the x-, y- and z-directions, respectively, p is the fluid pressure, p_c is the capillary pressure, k is the absolute permeability, μ is the viscosity, ρ is the density, s is the saturation, k_r is the relative permeability, g is the gravitational acceleration, t is the time, ϕ is the porosity, c_d is the concentration of the diffusive species, D_0 is the effective diffusion coefficient, and subscripts w and n denote the wetting phase and non-wetting phase, respectively.

We assumed that the wetting-phase density, ρ_w, is a linear function of the concentration of the diffusive species, c_{dw}:

$$\rho_w = \rho_{w0}(1 + b_c c_{dw}), \quad b_c = \frac{1}{\rho_w} \frac{\partial \rho_w}{\partial c_{dw}}, \tag{2.3a,b}$$

where ρ_{w0} is the density of the wetting phase at $c_{dw} = 0$ and b_c can be obtained from an equation of state.

The capillary pressure is a function of the phase saturations and can be obtained from the Leverett J-function (Leverett 1941):

$$J(s_w) = \frac{p_c}{(\rho_{w0} - \rho_n) g h} = \sqrt{\frac{k}{\phi}} \frac{p_c}{\wp \cos\theta}, \tag{2.4}$$

where $\wp$ is the surface tension between the non-wetting and wetting phase and θ is the contact angle between the fluid interfaces and the rock surface.

We used the height of capillary pressure, $h \sim \wp \cos\theta / (\rho_{w0} - \rho_n) g \sqrt{k/\phi}$, as a measure of the capillary force and adopted the van Genuchten–Mualem model for the relative permeabilities and capillary pressure relations (Mualem 1976; van Genuchten 1980):

$$k_{rn} = (1 - S)^{1/3} (1 - S^{1/m})^{2m}, \quad k_{rw} = S^{1/2} (1 - (1 - S^{1/m})^m)^2, \quad J = (S^{-1/m} - 1)^{1/n}, \tag{2.5a–c}$$

where $S = (s_w - s_{wr})/(1 - s_{wr})$, s_{wr} is the residual saturation of the wetting phase, $m = 1 - 1/n$ and $n > 1$ is the material parameter.

2.3. *Dimensionless formulation*

For the stability analysis, the domain bottom boundary, and hence the domain thickness H, has no effect on the initial development of instability because, at early times, when the diffusive boundary layer is very thin, the domain behaves as a semi-infinite medium in the z-direction. This allows us to use the ratio of diffusion to buoyancy velocity as an internal length scale (Riaz *et al.* 2006; Slim & Ramakrishnan 2010; Andres & Cardoso 2011; Emami-Meybodi 2017) for the stability problem under consideration. Hence, we chose $L_c = D_0 \varphi / u_b$ as the length scale, where $\varphi = \phi(1 - s_{wr})$ and $u_b = k g b_c \rho_{w0} c_d^* / \mu_w$ is

the buoyancy velocity. The length scale L_c is a measure of the thickness of the diffusive boundary layer at the time of instability, i.e. when the inhibiting effects of diffusion balance the driving effect of buoyancy on the development of fluid motion, making the solutal Rayleigh number of order unity. Thus, one can expect the onset of instability to be independent of H when $H/L_c \gg 1$.

We normalized the governing equations by choosing $D_0\varphi/u_b$ as the length scale and D_0/L_c^2 as the time scale. Accordingly, the dimensionless parameters are

$$t_D = \frac{D_0}{L_c^2}t, \quad x_D = \frac{x}{L_c}, \quad y_D = \frac{y}{L_c}, \quad z_D = \frac{z}{L_c}, \quad C = \frac{c}{c_d^*}, \quad U = \frac{u}{u_b}, \quad V = \frac{v}{u_b}, \quad W = \frac{w}{u_b}. \tag{2.6a–h}$$

As mentioned earlier, we considered a semi-infinite domain in the z-direction. The perturbations responsible for the diffusive boundary layer's instability are experimentally observed to originate within the layer near the solute–wetting phase interface at $z_D = 0$ (Spangenberg & Rowland 1961; Elder 1968; Blair & Quinn 1969; Wooding 1969; Green & Foster 1975). Thus, many studies approximate the vertical domain as semi-infinite and transform the vertical z-coordinate to the time-dependent variable $\xi(z, t) = z/\sqrt{Dt}$ to build initial perturbations that reflect experimental conditions (Ben, Demekhin & Chang 2002; Kim, Chung & Choi 2004; Riaz *et al.* 2006; Kim & Choi 2011; Meulenbroek, Farajzadeh & Bruining 2013). This transformation allows the flow fields to be expressed in terms of expansion functions localized within the diffusive boundary layer. Therefore, we chose a self-similar coordinate by applying the transformation $\xi = z_D/\sqrt{t_D}$ to localize the diffusion operator around the diffusive front and achieve considerable improvement in accuracy at early times. For the original layer geometry in a finite domain with a thickness of H (see figure 1), the parameter range over which the results are valid is given by $\delta(t_D) \sim \sqrt{t_D} \ll 1$, where δ is the penetration depth of the diffusive boundary layer within the wetting-phase region.

Using (2.6) and the ξ transformation, the dimensionless form of the governing equations for flow, wetting-phase saturation and concentration can be expressed as

$$\begin{aligned}
&\frac{\partial^2 W}{\partial x_D^2} + \frac{\partial^2 W}{\partial y_D^2} + \frac{1}{t_D}\frac{\partial^2 W}{\partial \xi^2} - k_{rw}\left(\cos\beta\left(\frac{\partial^2 C}{\partial x_D^2} + \frac{\partial^2 C}{\partial y_D^2}\right) + \sin\beta\frac{\partial^2 C}{\partial x_D \partial z_D}\right) \\
&\quad - k'_{rw}\left(\cos\beta\left(\frac{\partial S}{\partial x_D}\frac{\partial C}{\partial x_D} + \frac{\partial S}{\partial y_D}\frac{\partial C}{\partial y_D}\right) + \sin\beta\frac{\partial S}{\partial x_D}\frac{\partial C}{\partial z_D}\right) \\
&- \frac{k'_{rw}}{k_{rw}}\left(\frac{\partial W}{\partial x_D}\frac{\partial S}{\partial x_D} + \frac{\partial W}{\partial y_D}\frac{\partial S}{\partial y_D} + W\left(\frac{\partial^2 S}{\partial x_D^2} + \frac{\partial^2 S}{\partial y_D^2}\right) + \frac{1}{t_D}\frac{\partial S}{\partial \xi}\frac{\partial W}{\partial \xi} - \frac{1}{\sqrt{t_D}}\left(U\frac{\partial^2 S}{\partial x_D \partial \xi} + V\frac{\partial^2 S}{\partial y_D \partial \xi}\right)\right) \\
&\quad - \left(\frac{k'_{rw}}{k_{rw}}\right)'\left(W\left[\left(\frac{\partial S}{\partial y_D}\right)^2 + \left(\frac{\partial S}{\partial x_D}\right)^2\right] - \frac{1}{\sqrt{t_D}}\frac{\partial S}{\partial \xi}\left(U\frac{\partial S}{\partial x_D} + V\frac{\partial S}{\partial y_D}\right)\right) = 0,
\end{aligned} \tag{2.7a}$$

$$\begin{aligned}
&\frac{\partial S}{\partial t_D} - \frac{\xi}{2t_D}\frac{\partial S}{\partial \xi} - \frac{f'}{f}\left(U\frac{\partial S}{\partial x_D} + V\frac{\partial S}{\partial y_D} + \frac{W}{\sqrt{t_D}}\frac{\partial S}{\partial \xi}\right) \\
&+ \frac{G}{Bof}\left((k_{rn}J')'\left(\left(\frac{\partial S}{\partial x_D}\right)^2 + \left(\frac{\partial S}{\partial y_D}\right)^2 + \frac{1}{t_D}\left(\frac{\partial S}{\partial \xi}\right)^2\right) + k_{rn}J'\left(\frac{\partial^2 S}{\partial x_D^2} + \frac{\partial^2 S}{\partial y_D^2} + \frac{1}{t_D}\frac{\partial^2 S}{\partial \xi^2}\right)\right) \\
&+ \frac{\cos\beta}{f\sqrt{t_D}}\left(k_{rn}\frac{\partial C}{\partial \xi} + k'_{rn}(C+G)\frac{\partial S}{\partial \xi}\right) - \frac{\sin\beta}{f}\left(k_{rn}\frac{\partial C}{\partial x_D} + (C+G)k'_{rn}\frac{\partial S}{\partial x_D}\right) = 0
\end{aligned} \tag{2.7b}$$

and

$$S\frac{\partial C}{\partial t_D} - S\frac{\xi}{2t_D}\frac{\partial C}{\partial \xi} - \frac{\partial S}{\partial x_D}\frac{\partial C}{\partial x_D} - \frac{\partial S}{\partial y_D}\frac{\partial C}{\partial y_D} - \frac{1}{t_D}\frac{\partial S}{\partial \xi}\frac{\partial C}{\partial \xi} + U\frac{\partial C}{\partial x_D} + V\frac{\partial C}{\partial y_D} + \frac{W}{\sqrt{t_D}}\frac{\partial C}{\partial \xi} - S\left(\frac{\partial^2 C}{\partial x_D^2} + \frac{\partial^2 C}{\partial y_D^2} + \frac{1}{t_D}\frac{\partial^2 C}{\partial \xi^2}\right) = 0, \tag{2.7c}$$

where $f = M + k_{rn}/k_{rw}$, $M = \mu_n/\mu_w$ is the viscosity ratio and primes denote derivatives with respect to the saturation of the wetting phase.

As mentioned earlier, we considered the capillary transition zone combined with the underlying wetting-phase region as the domain of study. Accordingly, (2.7) is subject to the following conditions:

$$W(z_D = -1/Bo) = W(z_D = 0) = W(z_D \to \infty) = 0, \tag{2.8a}$$

$$V(z_D = -1/Bo) = V(z_D = 0) = V(z_D \to \infty) = 0, \tag{2.8b}$$

$$U(z_D = -1/Bo) = U(z_D \to \infty) = 0, \tag{2.8c}$$

$$S(z_D = -1/Bo) = 0, \quad S(z_D = 0) = S(z_D \to \infty) = 1, \tag{2.8d,e}$$

$$C(z_D = -1/Bo) = C(z_D = 0) = 1, \quad C(z_D \to \infty) = 0. \tag{2.8f,g}$$

According to (2.8), besides U at $z_D = 0$, other variables are subject to three known boundary conditions since the base state solutions for the capillary transition zone ($-1/B_o \le z_D \le 0$) and the wetting-phase region ($0 \le z_D \to \infty$) were obtained separately using the same boundary conditions at $z_D = 0$. Furthermore, U at $z_D = 0$ was obtained from the base state solution by applying the condition $U = 0$ when $C = 0$.

As noted from (2.7), the system under consideration can be explored with reference to the Bond number, $Bo = L_c/h$, gravity number, $G = k(\rho_{w0} - \rho_n)g/u_b\mu_w$, viscosity ratio, $M = \mu_n/\mu_w$, material parameter, n, and inclination angle, β.

Based on the schematic of the CO_2–water system shown in figure 1, the displacement takes place in the z-direction, and the denser fluid with the higher viscosity (water as the wetting phase) is located under the lighter fluid with the lower viscosity (CO_2 as the non-wetting phase). Such a two-phase system remains stable in the absence of solute diffusion into the wetting phase because $(\mu_w/k_{rw} - \mu_n/k_{rn})(U_0 - U_c)$ always remains a negative value (Marle 1981), where $U_c = k(\rho_{w0} - \rho_n)g/(\mu_w/k_{rw} - \mu_n/k_{rn})$ and U_0 is the base state advective velocity, which is zero for the problem under consideration. Therefore, G and M do not affect the instability of the two-phase system because the denser water with the higher viscosity is located under the lighter CO_2 with the lower viscosity (Emami-Meybodi 2017). In this study, we used fixed values of $G = 10$ and $M = 0.1$, representing the CO_2–water system.

The Bond number is a measure of the relative strength of gravitational forces to capillary forces where the limit $Bo \to \infty$ recovers the single-phase system in which $h \to 0$. The two-phase system can be divided into three categories based on the Bo value: buoyancy-dominant systems for $Bo > 10^2$; in-transition systems for $10^{-3} < Bo < 10^2$; and capillary-dominant systems for $Bo < 10^{-3}$ (Emami-Meybodi & Hassanzadeh 2013; Zhang & Emami-Meybodi 2018). We used a wide range of $10^{-3} \le Bo \le 10^3$ in this study to investigate the onset of instability for all three systems.

The material parameter $n > 1$ is a measure of the pore-size distribution, which depends on the degree of sorting of the grains in a porous medium. For the in-transition systems with $10^{-3} < Bo < 10^2$, the positive effect of the material

parameter on the onset of convection has been demonstrated using linear stability analysis (LSA; Zhang & Emami-Meybodi 2018) and direct numerical simulations (Emami-Meybodi & Hassanzadeh 2015). Larger values of n for in-transition systems reflect higher wetting-phase saturation just above the interface between the wetting and non-wetting phases, which means higher crossflow across the interface. Nonetheless, the material parameter has no significant influence on the onset of instability for the buoyancy-dominant and the capillary-dominant systems (Emami-Meybodi & Hassanzadeh 2013; Emami-Meybodi 2017; Zhang & Emami-Meybodi 2018). Considering prior investigations and the insignificant impact of the material parameter on the stability of buoyancy- and capillary-dominant systems, we used a fixed value of $n = 3$ ($\upsilon = 10$) in this study, where υ is a constant assigned according to the value of n that ensures $s_w = s_{wr}$ at $z = -h$.

3. Formulation of the stability problem

3.1. *Base state solutions*

We used the definition of the J-function $J = -(\cos\beta)Bo\, z_D$, (2.5*c*) and (2.8*d*,*e*) to obtain the base state solution for the wetting-phase saturation, S_0:

$$S_0(z_D) = 1 + \boldsymbol{H}(-z_D)[(1 + (-\upsilon(\cos\beta)Bo\, z_D)^n)^{(1-n)/n} - 1], \tag{3.1}$$

where $\boldsymbol{H}$ is the Heaviside step function with $\boldsymbol{H}(x) = 0$ for $x < 0$ and $\boldsymbol{H}(x) = 1$ for $x \geq 0$.

The base state solution for concentration (C_0) can be found from (2.7*c*) and (2.8*f*,*g*) using the Laplace transform (Farlow 1993)

$$C_0(z_D, t_D) = 1 - \boldsymbol{H}(z_D) erf\left(\frac{z_D}{2\sqrt{t_D}}\right). \tag{3.2}$$

According to (2.8*a*,*b*), the base state solutions for the velocity components of the wetting phase in the y- (V_0) and z-directions (W_0) are $W_0 = V_0 = 0$ since the system is initially subject to zero velocities in these directions. However, the velocity component in the x-direction varies with time and along the z-direction because of the wetting-phase saturation and density change in the capillary transition zone and the wetting-phase region, respectively. Hence, we first used (2.1*a*) for the wetting phase and (2.3*a*) to obtain the following differential equation for U_0:

$$\frac{\partial U_0}{\partial z_D} = \frac{k'_{rw}}{k_{rw}}\frac{\partial S_0}{\partial z_D}U_0 - k_{rw}\sin\beta\frac{\partial C_0}{\partial z_D}. \tag{3.3}$$

Equation (3.3) can be solved by applying (2.5) to get

$$U_0(z_D, t_D) = \boldsymbol{H}(z_D)(d_1 - (\sin\beta)C_0) + \boldsymbol{H}(-z_D)d_2\left(\psi\frac{(-\psi z_D)^{n-1} - ((-\psi z_D)^n + 1)^{(n-1)/n}}{((-\psi z_D)^n + 1)^{5(n-1)/4n}}\right)^2, \tag{3.4}$$

where $\psi = \upsilon(\cos\beta)Bo$ and d_1 and d_2 are constants that can be obtained by applying (2.8*c*,*g*) and $U_0 = 0$ at $C_0 = 0$ to (3.4):

$$d_1 = 0, \quad d_2 = -\frac{\sin\beta}{\psi^2}. \tag{3.5a,b}$$

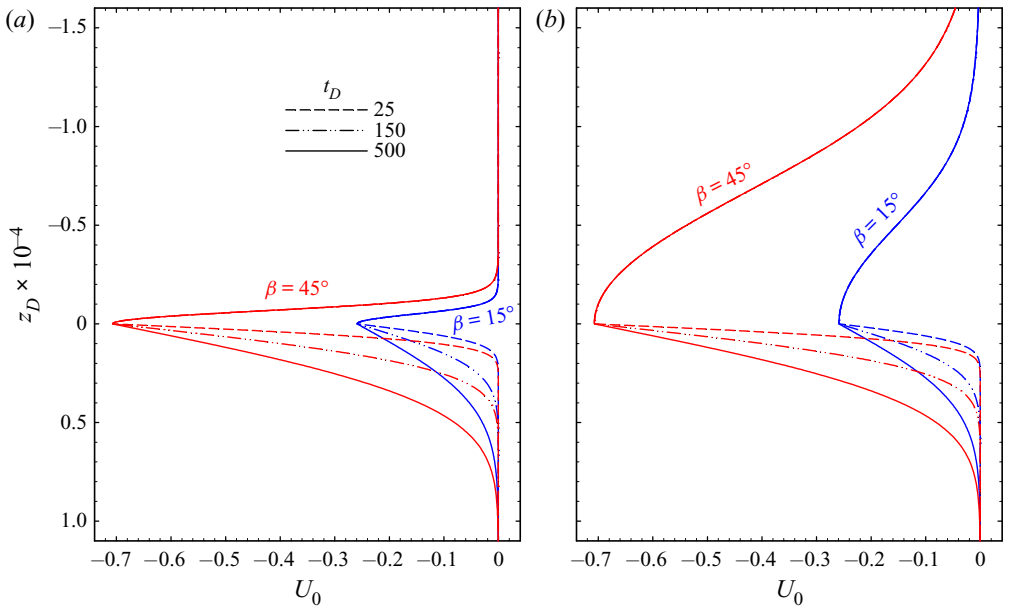

Figure 2. Base state velocity profiles along the z-direction from (3.6), for two inclined porous media having $\beta = 15°$ and 45° at $t_D = 25$, 150 and 500 with (*a*) $Bo = 0.01$ and (*b*) $Bo = 0.001$. Other parameters are fixed: $n = 3$ and $\upsilon = 10$.

Combining (3.4) and (3.5) gives

$$U_0(z_D, t_D) = -\sin\beta \left(\boldsymbol{H}(z_D) \left(erfc\left(\frac{z_D}{2\sqrt{t_D}} \right) \right) + \boldsymbol{H}(-z_D) \left(\frac{(-\psi z_D)^{n-1} - ((-\psi z_D)^n + 1)^{(n-1)/n}}{((-\psi z_D)^n + 1)^{5(n-1)/4n}} \right)^2 \right). \tag{3.6}$$

As noted from (3.6), the base state solution $U_0 = 0$ is recovered in the case of a horizontal porous medium, $\beta = 0°$ (Emami-Meybodi & Hassanzadeh 2013; Zhang & Emami-Meybodi 2018). Moreover, it is evident from these equations that the base state solution is left invariant by the transformation of $\beta \to \pi - \beta$ and $x \to -x$.

Figure 2 illustrates, for $Bo = 0.01$ and 0.001, how the velocity profiles vary along the z-direction for two inclined porous media having $\beta = 15°$ and 45° at $t_D = 25$, 150 and 500. The impact of inclination angle on the velocity values is evidenced in figure 2, where the magnitude of maximum velocity, $|U_{0,max}|$, increases from 0.25 to 0.7 by changing the inclination angle from 15° to 45°. A comparison between figure 2(*a*) and 2(*b*) shows that, while the $U_{0,max}$ and U_0 profiles within the wetting-phase region ($z_D > 0$) vary with β, they remain fixed with respect to Bo. However, the U_0 profile within the capillary transition zone ($z_D < 0$) is a function of both Bo and β. A good point is asking how such velocity behaviour is likely to affect the onset of natural convection. Stability analysis of the two-phase system is a valuable tool to find an answer.

3.2. *Linear stability analysis*

To conduct LSA, small disturbances of velocities U_1, V_1 and W_1, saturation S_1 and concentration C_1 were introduced; therefore, U, V, W, S and C can be written

as

$$\{U, V, W, S, C\}(x_D, y_D, \xi, t_D) = \{U_0, V_0, W_0, S_0, C_0\}(\xi, t_D) + \varepsilon\{U_1, V_1, W_1, S_1, C_1\}(\xi, t_D)\, \mathrm{e}^{\mathrm{i}(a_x x_D + a_y y_D)} + \text{c.c.}, \tag{3.7}$$

where $\mathrm{i} = \sqrt{-1}$ and a_x and a_y are the real-valued dimensionless components of the wavevector (i.e. wavenumbers in the x- and y-directions, respectively), with a very small amplitude ϵ. The subscripts 0 and 1 represent the base state and disturbance quantities, respectively.

Note that, for the stability problem under consideration, in the early stages of the diffusive boundary layer's formation, perturbations to the layer are damped. But eventually, a critical time for linear instability, τ_c, is reached, after which the vertical density gradient drives the fluid motion. We used the quasi-steady-state approximation (QSSA; Morton 1957; Lick 1965; Robinson 1976) to study such a linear regime and determine the critical time τ_c and its corresponding wavenumber α_c. QSSA assumes that the growth rate of perturbations is asymptotically faster than the evolution rate of the base state solutions, i.e. the diffusive boundary layer (Riaz *et al.* 2006; Daniel, Tilton & Riaz 2013). Thus, QSSA eliminates the time dependence of the base state by solving the perturbed equations at a frozen time τ. QSSA based on the frozen time τ has been widely applied to the solutal stability problem (Riaz *et al.* 2006; Selim & Rees 2007; Chan Kim & Kyun Choi 2012; Daniel *et al.* 2013; Emami-Meybodi & Hassanzadeh 2013; Tilton, Daniel & Riaz 2013; Kim 2015).

Accordingly, the concentration (3.2) and velocity (3.6) base state solutions are assumed frozen at $t_D = \tau$, and the stability of the frozen profiles is defined by

$$\{U_1, V_1, W_1, S_1, C_1\}(\xi, \tau) = \{U^*, V^*, W^*, S^*, C^*\}(\xi)\, \mathrm{e}^{\sigma\tau}, \tag{3.8}$$

where variables defined by asterisks represent the perturbation eigenfunctions and σ is the growth rate.

Introducing the perturbed solutions (3.7) and then applying QSSA (3.8) to (2.7) and retaining terms that are first-order in ϵ, the disturbance equations in the self-similar coordinates can be written as

$$\left(\frac{\partial^2}{\partial\xi^2} - \frac{k'_{rw}}{k_{rw}}\frac{\partial S_b}{\partial\xi}\frac{\partial}{\partial\xi} - \tilde{\alpha}^2\right) W^* + k_{rw}\left(\tilde{\alpha}^2\cos\beta - \mathrm{i}\gamma\tilde{\alpha}\sin\beta\frac{\partial}{\partial\xi}\right) C^* - \mathrm{i}\gamma\tilde{\alpha}(\sin\beta)k'_{rw}\frac{\partial C_0}{\partial\xi}S^* = 0, \tag{3.9a}$$

$$\begin{aligned}
&\sqrt{\tau}\frac{\partial S_0}{\partial\xi}\frac{f'}{f}W^* - \frac{\sqrt{\tau}}{f}\left(\cos\beta\left(k'_{rn}\frac{\partial S_0}{\partial\xi} + k_{rn}\frac{\partial}{\partial\xi}\right) - \mathrm{i}\gamma\tilde{\alpha}(\sin\beta)k_{rn}\right) C^* \\
&+\Bigg[\frac{\xi}{2}\frac{\partial}{\partial\xi} + \mathrm{i}\gamma\tilde{\alpha}\frac{\sqrt{\tau}}{f}k'_{rn}(\sin\beta)(G + C_0) - \frac{G}{Bo}\left(\begin{array}{l}\dfrac{k_{rn}J'}{f}\left(\dfrac{\partial^2}{\partial\xi^2} - \tilde{\alpha}^2\right) + 2\dfrac{(k_{rn}J')'}{f}\dfrac{\partial S_0}{\partial\xi}\dfrac{\partial}{\partial\xi} \\ \quad + \left(\dfrac{k_{rn}J'}{f}\right)'\dfrac{\partial^2 S_0}{\partial\xi^2} + \left(\dfrac{(k_{rn}J')'}{f}\right)'\left(\dfrac{\partial S_0}{\partial\xi}\right)^2\end{array}\right) \\
&-(\cos\beta)\sqrt{\tau}\left((G + C_0)\left(\frac{k'_{rn}}{f}\frac{\partial}{\partial\xi} + \left(\frac{k'_{rn}}{f}\right)'\frac{\partial S_0}{\partial\xi}\right) + \left(\frac{k_{rn}}{f}\right)'\frac{\partial C_0}{\partial\xi}\right)\Bigg] S^* - \tilde{\sigma}S^* = 0
\end{aligned} \tag{3.9b}$$

and

$$-\frac{\sqrt{\tau}}{S_0}\frac{\partial C_0}{\partial \xi}W^* + \frac{1}{S_0}\frac{\partial C_0}{\partial \xi}\frac{\partial S^*}{\partial \xi} + \left(\frac{\partial^2}{\partial \xi^2} + \left(\frac{\xi}{2} + \frac{1}{S_0}\frac{\partial S_0}{\partial \xi}\right)\frac{\partial}{\partial \xi} - \tilde{\alpha}^2\right)C^* - \tilde{\sigma}C^* = 0, \tag{3.9c}$$

where $\tilde{\sigma} = \sigma\tau$, $\tilde{\alpha} = \alpha\sqrt{\tau}$ and $\alpha = \sqrt{a_x^2 + a_y^2}$ is the horizontal wavenumber. A new parameter $\gamma = a_x/\alpha$ is defined in (3.9) as $\gamma \in [0, 1]$. The special cases $\gamma = 0$ and $\gamma = 1$ lead to longitudinal and transverse rolls, respectively, while $0 < \gamma < 1$ defines oblique rolls. Moreover, the relative permeabilities and capillary pressure in (2.7) were decomposed using the first-order Taylor expansion $\{k_r, J\} = \{k_r, J\}(S_0) + S_1\{k_r, J\}'$.

System (3.9) may be regarded as an eigenvalue problem for complex growth rate, $\sigma = \mathrm{Re}(\sigma) + \mathrm{i}\,\mathrm{Im}(\sigma)$, as a function of α, γ, β, τ and Bo, where Re and Im denote the real and imaginary parts, respectively, of a complex number. The imaginary part of σ defines the angular frequency, whereas the real part determines the unstable (if $\mathrm{Re}(\sigma) > 0$) or stable (if $\mathrm{Re}(\sigma) < 0$) nature of the system. Since this study focuses on the neutral stability analysis, one considers $\mathrm{Re}(\sigma) = 0$. Accordingly, σ is purely imaginary at onset and system (3.9) may instead be regarded as an eigenvalue problem for both τ and $\mathrm{Im}(\sigma)$ as a function of α, γ, β and Bo.

3.3. *Computational domain discretization*

We discretized (3.9) using a finite-difference technique in which a three-point centred Lagrange polynomial approximation was used for numerical differentiation (Singh & Bhadauria 2009). A non-uniform grid system was employed to choose finer grids in the vicinity $\xi = 0$. The non-uniform grid spacing was obtained by $\Delta\xi_j = \chi^j / \sum_{k=1}^{N} \chi^k$ where $N = 1000$ is the number of grid blocks, $\chi = 1.007$ is the mesh increment rate and j refers to the grid spacing index, which starts from 1 for the first grid interval at the top boundary and ends with 1000 for the last grid interval at the bottom boundary. The resulting discretized system of equations (3.9) can be expressed by a system of linear equations:

$$\boldsymbol{q}_1\boldsymbol{W}^* + \boldsymbol{q}_2\boldsymbol{S}^* + \boldsymbol{q}_3\boldsymbol{C}^* = 0, \tag{3.10a}$$

$$\boldsymbol{q}_4\boldsymbol{W}^* + (\boldsymbol{q}_5 - \tilde{\sigma}\boldsymbol{I})\boldsymbol{S}^* + \boldsymbol{q}_6\boldsymbol{C}^* = 0, \tag{3.10b}$$

$$\boldsymbol{q}_7\boldsymbol{W}^* + \boldsymbol{q}_8\boldsymbol{S}^* + (\boldsymbol{q}_9 - \tilde{\sigma}\boldsymbol{I})\boldsymbol{C}^* = 0, \tag{3.10c}$$

where $\boldsymbol{W}^*$, $\boldsymbol{S}^*$ and $\boldsymbol{C}^*$ are the eigenvectors for the vertical components of velocity, saturation and concentration, respectively, $q_1 - q_9$ are the discretization operators related to the eigenfunctions, and $\boldsymbol{I}$ is the identity matrix. System (3.10) can be simplified by substituting (3.10*a*) into (3.10*b*,3.10*c*) to give

$$\begin{bmatrix} \boldsymbol{q}_5 - \boldsymbol{q}_4\boldsymbol{q}_1^{-1}\boldsymbol{q}_2 - \tilde{\sigma}\boldsymbol{I} & \boldsymbol{q}_6 - \boldsymbol{q}_4\boldsymbol{q}_1^{-1}\boldsymbol{q}_3 \\ \boldsymbol{q}_8 - \boldsymbol{q}_7\boldsymbol{q}_1^{-1}\boldsymbol{q}_2 & \boldsymbol{q}_9 - \boldsymbol{q}_7\boldsymbol{q}_1^{-1}\boldsymbol{q}_3 - \tilde{\sigma}\boldsymbol{I} \end{bmatrix} \begin{bmatrix} \boldsymbol{S}^* \\ \boldsymbol{C}^* \end{bmatrix} = \begin{bmatrix} 0 \\ 0 \end{bmatrix}. \tag{3.11}$$

System (3.11) constitutes a linear algebraic eigenvalue problem, which can be numerically solved for $\tilde{\sigma}$ using standard techniques (Lin & Segel 1988) once α, γ, β, τ and Bo are prescribed.

3.4. *Calculation of τ and α*

The previous section described how to obtain the growth rate σ, or the angular frequency $\mathrm{Im}(\sigma)$, by solving (3.11) from given values of α, γ, β, τ and Bo. But an additional step

must be incorporated to draw neutral stability curves. This involves calculating τ and α from a given configuration with known γ, β and Bo. We carried out this step by enforcing a condition that $\mathrm{Re}(\sigma) = 0$, thus satisfying the neutral stability requirement. In the MATLAB code developed, this is accomplished by incorporating the secant method (Chapra & Canale 2010) to find the values of τ and α that satisfy $\mathrm{Re}(\sigma) = 0$. Furthermore, the largest eigenvalues and the corresponding eigenvectors of (3.11) were obtained to determine the critical time τ_c and its corresponding wavenumber α_c. In other words, the evolution of the maximum value of the concentration, the saturation or the velocity eigenfunction forms the basis of the growth rate at given τ and α. The dynamical system is said to be stable if $\mathrm{Re}(\sigma) < 0$ and a critical time τ_c (the onset of instability) is indicated when the growth rate just becomes positive at a critical wavenumber α_c.

4. Results and discussion

We performed LSA by solving (3.11) to parametrize the effect of inclination of a saturated porous layer subject to a capillary transition zone on the growth rate of perturbations and, consequently, the onset of natural convection. We conducted LSA for a wide range of $0 \leq \gamma \leq 1$, $0° \leq \beta \leq 90°$ and $10^{-3} \leq Bo \leq 10^{3}$ but at fixed values of $G = 10$, $M = 0.1$ and $n = 3$. In what follows, first, the neutral stability curves for the longitudinal ($\gamma = 0$), oblique ($\gamma = 0.5$) and transverse ($\gamma = 1$) rolls are discussed. Then, critical values for the onset of the instability (α_c, τ_c) are obtained by seeking the minimum of the neutral stability function $\tau(\alpha)$.

4.1. *Neutral stability curves*

The first results are focused on the neutral stability curves for the longitudinal ($\gamma = 0$), oblique ($\gamma = 0.5$) and transverse ($\gamma = 1$) rolls. Figure 3 depicts the neutral stability curves in the plane (α, τ) with β from 0° to 45° for longitudinal rolls $\gamma = 0$. We considered a buoyancy-dominant system with $Bo = 10^{3}$ (negligible capillary transition zone), a capillary-dominant system with $Bo = 10^{-3}$ (considerable capillary transition zone) and two in-transition systems with $Bo = 0.1$ and 0.01. As shown in figure 4, at a given Bo, the neutral stability curve is shrunken and shifted upwards as β increases from 0° to 45°, revealing the stabilizing effect of the inclination on the onset of instability. As one can observe from comparing these curves at different Bo, when the Bond number is very small, the neutral stability curves are less sensitive to the inclination angle. Conversely, for a larger value of Bo, the neutral stability curves move upwards significantly as β increases, thus describing the stronger impact of β in stabilizing the diffusive boundary layer in the buoyancy-dominant systems than in the capillary-dominant systems. When β becomes as small as 5°, the neutral stability curves behave very similarly to the horizontal case ($\beta = 0$), particularly for the systems with significantly small Bond numbers, i.e. $Bo \to 0$. We note that the neutral stability curves of the longitudinal rolls ($\gamma = 0$) for the horizontal cases are identical to the results presented by Emami-Meybodi (2017) and Zhang & Emami-Meybodi (2018).

Figure 4 displays neutral stability curves for oblique rolls $\gamma = 0.5$ in the plane (α, τ) with different inclination angles at $Bo = 10^{3}$, 10^{-1}, 10^{-2} and 10^{-3}. This figure shows that the neutral stability curves shrink and move upwards as the inclination angle increases, with larger changes for the oblique rolls than for the longitudinal rolls. This phenomenon becomes significant in the buoyancy-dominant systems having high values of Bond numbers.

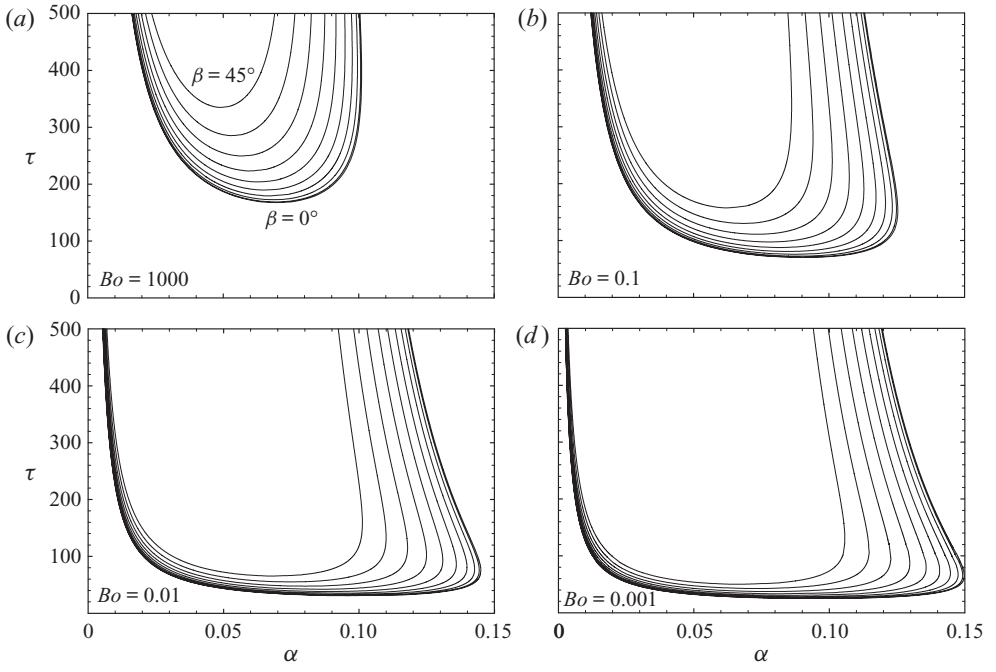

Figure 3. Neutral stability curves in the plane (α, τ) with different Bond numbers $Bo = 10^3$, 10^{-1}, 10^{-2} and 10^{-3}, and for different inclination angles, β, from 0° to 45° in increments of 5° for longitudinal rolls $\gamma = 0$.

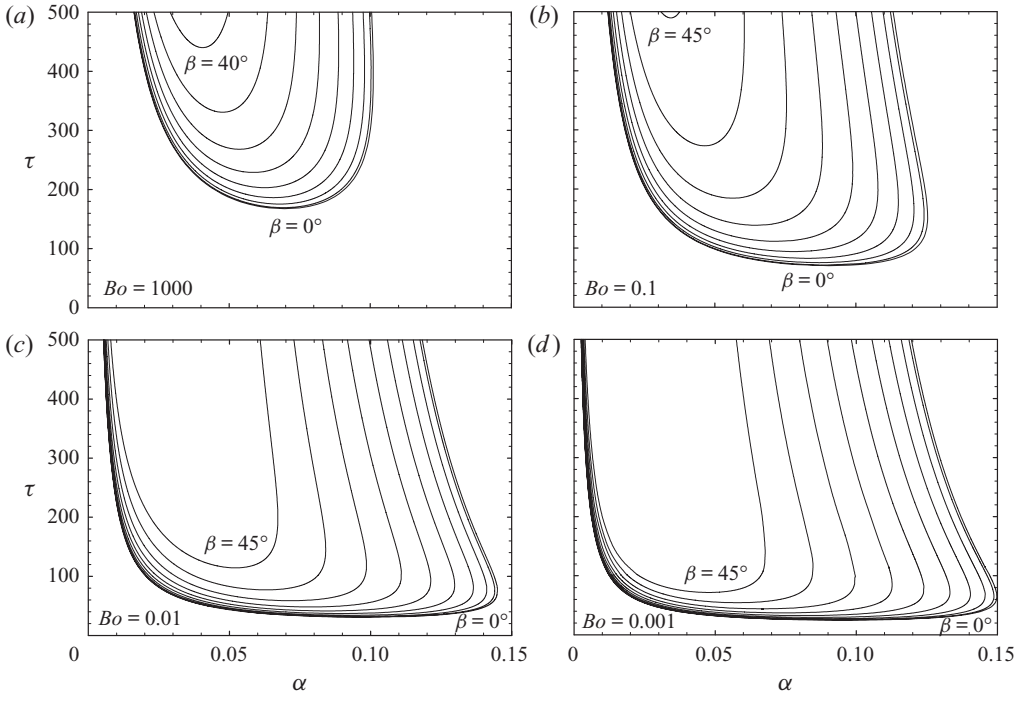

Figure 4. Neutral stability curves in the plane (α, τ) with different Bond numbers $Bo = 10^3$, 10^{-1}, 10^{-2} and 10^{-3}, and for different inclination angles, β, from 0° to 45° in increments of 5° for oblique rolls $\gamma = 0.5$.

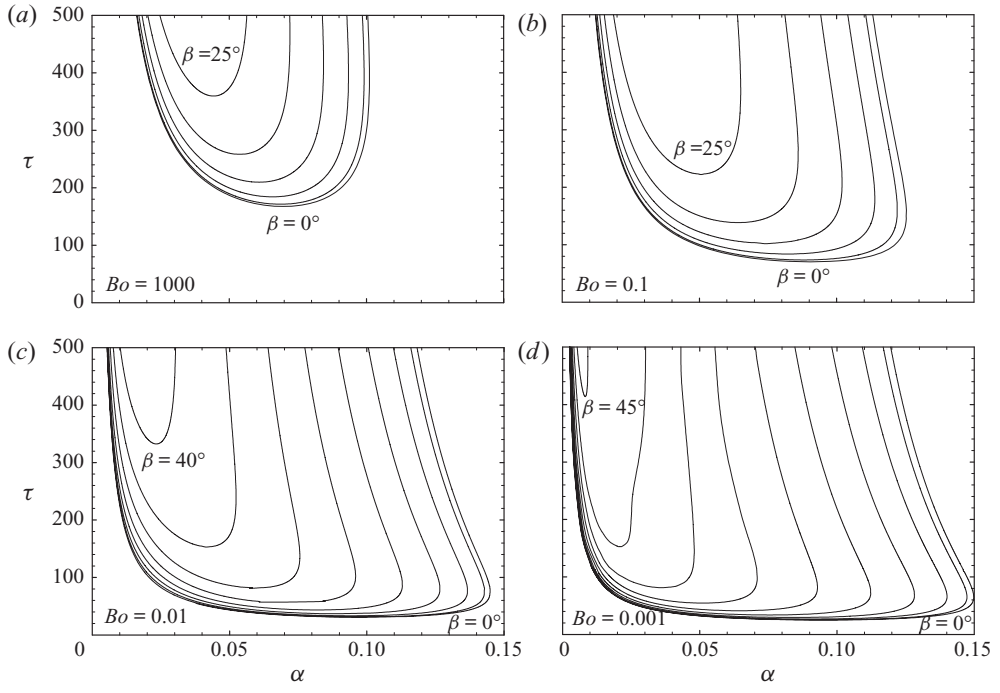

Figure 5. Neutral stability curves in the plane (α, τ) with different Bond numbers $Bo = 10^3$, 10^{-1}, 10^{-2} and 10^{-3}, and for different inclination angles, β, from 0° to 45° in increments of 5° for transverse rolls $\gamma = 1$.

Figure 5 refers to transverse rolls and displays neutral stability curves in the plane (α, τ) with different inclination angles at $Bo = 10^3$, 10^{-1}, 10^{-2} and 10^{-3}. A comparison between this figure and figures 3 and 4, within the shown vertical range, reveals that the transverse rolls are the least unstable rolls, where the natural stability curves are significantly shifted upwards. This occurrence is further intensified at high values of Bo, so that, for sufficiently large Bond numbers and a sufficiently large inclination angle. If the inclination is sufficiently high (e.g. $\beta = 30$ for the buoyancy-dominant systems and $\beta = 50$ for the capillary-dominant systems), the curves for larger values of β move upwards to such an extent that they are no longer visible within the vertical range of the plots.

4.2. *Critical values*

After examining the neutral stability curves, the next results are focused on the critical values of time and wavenumber. Figure 6 shows the critical time and its associated critical wavenumber as functions of the inclination angle at different $Bo = 10^3$, 10^{-1}, 10^{-2} and 10^{-3}, which have been obtained by minimizing time over all wavenumbers as β increases. This figure illustrates that, at a given Bo, the critical time increases with β, whereas the critical wavenumber decreases with β. It is also interesting to note that, for small inclination angles, the dependence on β is minor, which is further reduced for smaller values of Bo. Conversely, for sufficiently large inclination angles, when $\beta > 60°$, the onset of instability sharply increases with β. In fact, at very large inclination angles, and as $\beta \to 90°$, there is no dependence on Bo and there are no unstable longitudinal rolls since $\tau_c \to \infty$ and $\alpha_c \to 0$.

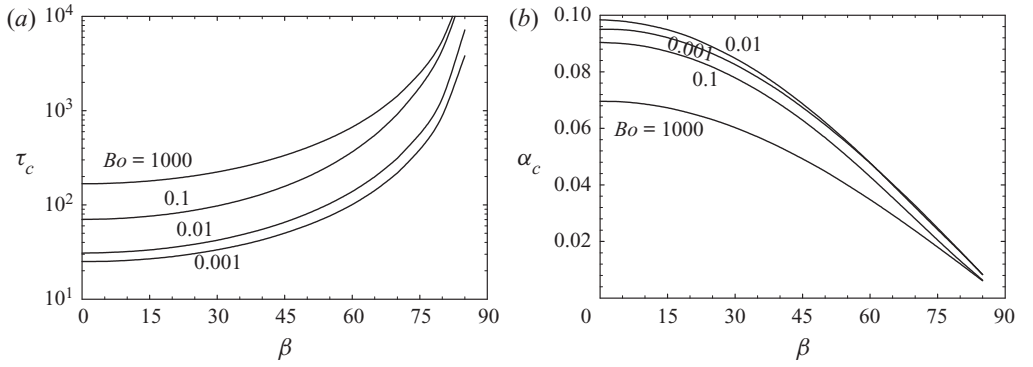

Figure 6. Critical time τ_c and its corresponding wavenumber α_c curves versus β at different Bond numbers $Bo = 10^3$, 10^{-1}, 10^{-2} and 10^{-3} for longitudinal rolls $\gamma = 0$.

Further investigation of LSA results shows that, for $\beta \leq 60°$, the critical dimensionless time and corresponding wavenumber vary exponentially with β. After testing several different exponential models, we found that for both buoyancy-dominant ($Bo = 10^3$) and capillary-dominant ($Bo = 10^{-3}$) systems, when $\beta \leq 60°$, the critical values follow the Stirling model for the onset of instability and its corresponding wavenumber:

$$\tau_c = \tau_{c0}[1 + 0.045(e^{0.07\beta} - 1)], \tag{4.1a}$$

$$\alpha_c = \alpha_{c0}[1 - 0.077(e^{0.034\beta} - 1)], \tag{4.1b}$$

where τ_{c0} and α_{c0} are the critical time and wavenumber for the horizontal case ($\beta = 1$). For the buoyancy-dominant horizontal systems, the critical time and wavenumber are $\tau_{c0} = 167.6$ and $\alpha_{c0} = 0.0696$, respectively; and, for the capillary-dominant horizontal systems, the critical values are $\tau_{c0} = 25.1$ and $\alpha_{c0} = 0.095$. These results are consistent with the results presented by Emami-Meybodi (2017) and Zhang & Emami-Meybodi (2018).

We have analysed the stability of the diffusive boundary layer in a semi-infinite domain. This analysis is applicable to a finite domain when the penetration depth of the diffusive boundary layer is small relative to the domain thickness. Hence, the critical time and wavenumber relationships (4.1) apply only when $\delta \sim \sqrt{t_D} \ll 1$.

Figure 7 displays the critical time and the associated wavenumber for oblique rolls, ranging from longitudinal ($\gamma = 0$, red curves) to transverse ($\gamma = 1$, blue curves), under different inclination angles of the porous medium for the buoyancy-dominant and capillary-dominant systems. As one can infer from the critical time plots, the longitudinal rolls are the most unstable, as the lowest curves are those with $\gamma = 0$. Accordingly, the highest curves in the critical time plots represent the transverse rolls, which are the most stable rolls. As expected, the critical wavenumber curves move downwards as the inclination angle increases, which implies that the number of convective rolls decreases as γ increases.

5. Summary and conclusions

We examined the effect of inclination on the stability of solutal convection in the presence of a capillary transition zone by considering a three-dimensional, two-phase, two-component, partially miscible system, where a non-wetting solute diffuses into an underlying inclined porous layer that is initially saturated with a wetting phase.

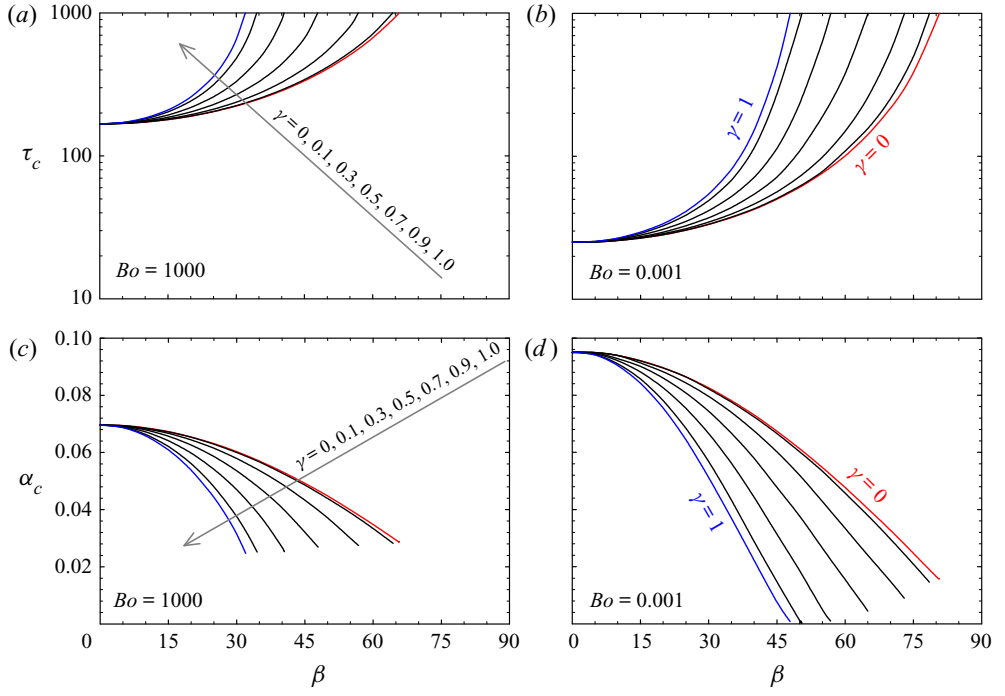

Figure 7. Critical time τ_c and its corresponding wavenumber α_c curves versus β at different $\gamma = 0$ (red curves), 0.1, 0.3, 0.5, 0.7, 0.9, 0.9, 1.0 (blue curves) for the buoyancy-dominant ($Bo = 10^3$) and capillary-dominant ($Bo = 10^{-3}$) systems.

We assumed that gravity–capillary equilibration establishes a capillary transition zone between the wetting and non-wetting regions. The diffusion of solute into the wetting phase creates a dense boundary layer beneath the capillary transition zone. While the diffusive boundary layer becomes unstable, the gravity-driven flow that arises from the variation of wetting-phase density across the layer may delay the onset of natural convection. Accordingly, the base state of the problem under consideration deals with transient concentration and velocity profiles. We derived a gravity-driven flow equation for the transient velocity field of the wetting phase, which is a function of the material parameter n, Bond number Bo and inclination angle β. After conducting LSA using the QSSA, we obtained a differential eigenvalue problem composed of a system of three complex-valued equations, which are a function of the dimensionless wavenumber α, dimensionless time τ, wavenumber ratio γ, Bond number Bo and inclination angle β. The differential equations were discretized using the three-point centred scheme of finite-difference technique and solved numerically to determine the critical times, critical wavenumbers and neutral stability curves as a function of β at different Bo.

We first analysed the neutral stability curves for different inclination angles and different Bond numbers, as well as for longitudinal, oblique and transverse rolls. The results have been presented for three two-phase systems: buoyancy-dominant when $Bo > 10^2$, in-transition when $10^{-3} < Bo < 10^2$ and capillary-dominant when $\mathrm{Bo} < 10^{-3}$. The results reveal the stabilizing effect of the inclination on the onset of instability. This stabilization effect intensifies from capillary-dominant to buoyancy-dominant systems. Further, it was

shown that the natural stability curves are the lowest in the plane (α, τ) for longitudinal rolls at any given β and Bo, indicating that they are the most unstable ones.

The analysis of stability carried out under the assumption of a perfectly horizontal porous layer leads to the conclusion that instability takes place if τ exceeds its critical value, which depends on Bo: for the buoyancy-dominant systems, $\tau_{c0} = 167.6$ and $\alpha_{c0} = 0.0696$, and for the capillary-dominant systems, $\tau_{c0} = 25.1$ and $\alpha_{c0} = 0.095$. Relaxing the assumption of a perfectly horizontal porous medium implies that even a small inclination could be sufficient to stabilize the diffusive boundary layer and significantly delay the onset of instability, particularly in buoyancy-dominant systems. For both buoyancy-dominant and capillary-dominant systems with $\beta \leq 60°$, the critical values follow the Stirling model $\tau_c/\tau_{c0} = 1 + 0.045(e^{0.07\beta} - 1)$ and $\alpha_c/\alpha_{c0} = 1–0.077(e^{0.034\beta} - 1)$ for time and associated wavenumber, respectively. For $\beta > 60°$, the onset of instability sharply increases with the inclination angle, and when $\beta \to 90°$, there are no unstable longitudinal rolls as $\tau_c \to \infty$ and $\alpha_c \to 0$ independently of the Bond number values.

The findings of this study have an important implication not only in various scientific and engineering disciplines, such as carbon dioxide sequestration in deep saline aquifers, but also for experimental research, as it shows that a perfect alignment must be employed for horizontal natural convection experiments to avoid the stabilizing effect of gravity-driven flow, in particular for buoyancy-dominant systems. While the focus of this study was on the development of an LSA, it will be extended to nonlinear analysis in future studies by conducting direct numerical simulations to examine the effect of inclination angle combined with the capillary transition zone on the onset of convection and subsequent convective mixing.

Funding. This research has been enabled with financial support from the Penn State Institute of Energy and the Environment (PSIEE) and with the use of computing resources provided by the Institute for CyberScience (ICS) at the Pennsylvania State University. The second author acknowledges the support by the Science Foundation of China University of Petroleum, Beijing (No. 2462021BJRC003).

Declaration of interests. The authors report no conflict of interest.

Author ORCIDs.
Hamid Emami-Meybodi https://orcid.org/0000-0002-3706-2710;
Fengyuan Zhang https://orcid.org/0000-0003-2482-6440.

References

Andres, J.T.H. & Cardoso, S.S. 2011 Onset of convection in a porous medium in the presence of chemical reaction. *Phys. Rev.* E **83** (4), 046312.

Aziz, K. & Settari, A. 1979 *Petroleum reservoir simulation*. Applied Science Publication Ltd.

Barletta, A. & Storesletten, L. 2011 Thermoconvective instabilities in an inclined porous channel heated from below. *Intl J Heat Mass Transfer* **54** (13–14), 2724–2733.

Ben, Y., Demekhin, E.A. & Chang, H.-C. 2002 A spectral theory for small-amplitude miscible fingering. *Phys. Fluids* **14** (3), 999–1010.

Blair, L.M. & Quinn, J. 1969 The onset of cellular convection in a fluid layer with time-dependent density gradients. *J. Fluid Mech.* **36** (2), 385–400.

Bolster, D. 2014 The fluid mechanics of dissolution trapping in geologic storage of CO_2. *J. Fluid Mech.* **740**, 1–4.

Bories, S. & Combarnous, M. 1973 Natural convection in a sloping porous layer. *J. Fluid Mech.* **57** (1), 63–79.

Chan Kim, M. & Kyun Choi, C. 2012 Linear stability analysis on the onset of buoyancy-driven convection in liquid-saturated porous medium. *Phys. Fluids* **24** (4), 044102.

Chapra, S.C. & Canale, R.P. 2010 *Numerical methods for engineers*. McGraw-Hill Higher Education.

Chen, Z., Huan, G. & Ma, Y. 2006 *Computational methods for multiphase flows in porous media*. Siam.

DANIEL, D., RIAZ, A. & TCHELEPI, H.A. 2015 Onset of natural convection in layered aquifers. *J. Fluid Mech.* **767**, 763–781.

DANIEL, D., TILTON, N. & RIAZ, A. 2013 Optimal perturbations of gravitationally unstable, transient, boundary layers in porous media. *J. Fluid Mech.* **727**, 456–487.

ELDER, J. 1968 The unstable thermal interface. *J. Fluid Mech.* **32** (1), 69–96.

ELENIUS, M.T., NORDBOTTEN, J.M. & KALISCH, H. 2012 Effects of a capillary transition zone on the stability of a diffusive boundary layer. *IMA J. Appl. Maths* **77** (6), 771–787.

EMAMI-MEYBODI, H. 2017 Stability analysis of dissolution-driven convection in porous media. *Phys. Fluids* **29** (1), 014102.

EMAMI-MEYBODI, H. & HASSANZADEH, H. 2013 Stability analysis of two-phase buoyancy-driven flow in the presence of a capillary transition zone. *Phys. Rev.* E **87** (3), 033009.

EMAMI-MEYBODI, H. & HASSANZADEH, H. 2015 Two-phase convective mixing under a buoyant plume of CO_2 in deep saline aquifers. *Adv. Water Resour.* **76**, 55–71.

EMAMI-MEYBODI, H., HASSANZADEH, H., GREEN, C.P. & ENNIS-KING, J. 2015 Convective dissolution of CO_2 in saline aquifers: Progress in modeling and experiments. *Intl J. Greenh. Gas Control* **40**, 238–266.

ENNIS-KING, J.P. & PATERSON, L. 2005 Role of convective mixing in the long-term storage of carbon dioxide in deep saline formations. *SPE J.* **10** (03), 349–356.

FARLOW, S.J. 1993 *Partial differential equations for scientists and engineers*. Courier Corporation.

GHESMAT, K., HASSANZADEH, H. & ABEDI, J. 2011 The impact of geochemistry on convective mixing in a gravitationally unstable diffusive boundary layer in porous media: CO_2 storage in saline aquifers. *J. Fluid Mech.* **673**, 480–512.

GREEN, L.L. & FOSTER, T.D. 1975 Secondary convection in a Hele Shaw cell. *J. Fluid Mech.* **71** (4), 675–687.

HASSANZADEH, H., POOLADI-DARVISH, M. & KEITH, D. 2005 Modelling of convective mixing in CO_2 storage. *J. Can. Petrol. Technol.* **44** (10), 43–51.

HASSANZADEH, H., POOLADI-DARVISH, M. & KEITH, D.W. 2007 Scaling behavior of convective mixing, with application to geological storage of CO_2. *AIChE J.* **53** (5), 1121–1131.

HORTON, C. & ROGERS, F. JR. 1945 Convection currents in a porous medium. *J. Appl. Phys.* **16** (6), 367–370.

KIM, M.C. 2015 The effect of boundary conditions on the onset of buoyancy-driven convection in a brine-saturated porous medium. *Trans. Porous Med.* **107** (2), 469–487.

KIM, M.C. & CHOI, C.K. 2011 The stability of miscible displacement in porous media: nonmonotonic viscosity profiles. *Phys. Fluids* **23** (8), 084105.

KIM, M.C., CHUNG, T.J. & CHOI, C.K. 2004 Onset of buoyancy-driven convection in the horizontal fluid layer heated from below with time-dependent manner. *Korean J. Chem. Engng* **21** (1), 69–74.

LAPWOOD, E. 1948 *Convection of a fluid in a porous medium*. Mathematical Proceedings of the Cambridge Philosophical Society. **44** (4), 508–521.

LEVERETT, M. 1941 Capillary behavior in porous solids. *Trans. AIME* **142** (01), 152–169.

LICK, W. 1965 The instability of a fluid layer with time-dependent heating. *J. Fluid Mech.* **21** (3), 565–576.

LIN, C.-C. & SEGEL, L.A. 1988 *Mathematics applied to deterministic problems in the natural sciences*. Siam.

MARLE, C. 1981 *Multiphase flow in porous media*. Éditions Technip.

MEULENBROEK, B., FARAJZADEH, R. & BRUINING, H. 2013 The effect of interface movement and viscosity variation on the stability of a diffusive interface between aqueous and gaseous CO_2. *Phys. Fluids* **25** (7), 074103.

MORTON, B. 1957 On the equilibrium of a stratified layer of fluid. *Q. J. Mech. Appl. Maths* **10** (4), 433–447.

MUALEM, Y. 1976 Hysteretical models for prediction of the hydraulic conductivity of unsaturated porous media. *Water Resour. Res.* **12** (6), 1248–1254.

NIELD, D.A. & BEJAN, A. 2017 *Convection in porous media*. Springer.

REES, D.A.S. & BASSOM, A. 2000 The onset of Darcy-Bénard convection in an inclined layer heated from below. *Acta Mechanica* **144** (1–2), 103–118.

REES, D.A.S., STORESLETTEN, L. & POSTELNICU, A. 2006 The onset of convection in an inclined anisotropic porous layer with oblique principle axes. *Trans. Porous Med.* **62** (2), 139–156.

RIAZ, A., HESSE, M., TCHELEPI, H. & ORR, F. 2006 Onset of convection in a gravitationally unstable diffusive boundary layer in porous media. *J. Fluid Mech.* **548**, 87–111.

ROBINSON, J. 1976 Theoretical analysis of convective instability of a growing horizontal thermal boundary layer. *Phys. Fluids* **19** (6), 778–791.

SELIM, A. & REES, D.A.S. 2007 The stability of a developing thermal front in a porous medium. I. Linear theory. *J. Porous Med.* **10** (1), 1–16.

SINGH, A.K. & BHADAURIA, B. 2009 Finite difference formulae for unequal sub-intervals using Lagrange's interpolation formula. *Intl J. Math. Anal.* **3** (17), 815–827.

SLIM, A.C. 2014 Solutal-convection regimes in a two-dimensional porous medium. *J. Fluid Mech.* **741**, 461–491.

SLIM, A.C. & RAMAKRISHNAN, T.S. 2010 Onset and cessation of time-dependent, dissolution-driven convection in porous media. *Phys. Fluids* **22** (12), 124103.

SPANGENBERG, W. & ROWLAND, W. 1961 Convective circulation in water induced by evaporative cooling. *Phys. Fluids* **4** (6), 743–750.

SPHAIER, L., BARLETTA, A. & CELLI, M. 2015 Unstable mixed convection in a heated inclined porous channel. *J. Fluid Mech.* **778**, 428–450.

TILTON, N., DANIEL, D. & RIAZ, A. 2013 The initial transient period of gravitationally unstable diffusive boundary layers developing in porous media. *Phys. Fluids* **25** (9), 092107.

VAN GENUCHTEN, M.T. 1980 A closed-form equation for predicting the hydraulic conductivity of unsaturated soils 1. *Soil Sci. Soc. Am. J.* **44** (5), 892–898.

WEBER, J.E. 1974 Thermal convection in a tilted porous layer. Preprint series. Mechanics and Applied Mathematics. Available at: http://urn.nb.no/URN:NBN:no-23418.

WOODING, R.A. 1969 Growth of fingers at an unstable diffusing interface in a porous medium or Hele-Shaw cell. *J. Fluid Mech.* **39** (3), 477–495.

ZHANG, F. & EMAMI-MEYBODI, H. 2018 Instability of a diffusive boundary layer beneath a capillary transition zone. *Fluids* **3** (4), 85.